Molecular Dynamics in the Solid State. The Order–Disorder Transition of Monoclinic Sulfur

Larry M. Goldsmith and Charles E. Strouse*

Contribution No. 3831 from the Department of Chemistry, University of California, Los Angeles, California 90024. *Received May 16, 1977*

Abstract: Multiple-temperature x-ray structural analysis is demonstrated to be a powerful probe of molecular dynamics in the solid state. Complete x-ray crystal structure determinations are reported for monoclinic (β) sulfur at five temperatures in the range 113–218 K. These determinations allow detailed examination of the thermodynamic, dynamic, and mechanistic properties of the structural transformation from an ordered state to a state in which one-third of the S_8 molecules are twofold disordered. The transition is cooperative with T_c = 198 K. Critical scattering observed above T_c and the temperature dependence of the long-range order parameter just below T_c are both indicative of three-dimensional order. Analysis of the temperature dependence of the long-range order parameter in the low-temperature limit provides an ordering energy of 1.1 kcal/mol. Lattice energy calculations based on the crystallographic data yield an upper bound of 5 kcal/mol for the barrier between the two sites. These calculations indicate that the pathway consisting of a simple, independent molecular rotation is a significant contributor to the overall transformation mechanism. The calculated energy surface in the vicinity of the two minima is found to be consistent with the crystallographically observed thermal motion. Crystal data: $P2_1$, Z = 6; at 113 K a = 10.799 (2), b = 10.684 (2), c = 10.663 (2) Å, β = 95.71 (1)° (λ 0.71069).

While solid state phase transitions in metallic alloys have been investigated extensively with powder x-ray diffraction methods, relatively little use has been made of more powerful single-crystal structural techniques in the elucidation of the energetics and dynamics of phase transitions in molecular solids. For the large class of crystalline materials that undergo continuous structural transformations over a range of temperature, multiple-temperature x-ray structure determination can provide a detailed picture of the molecular process involved in the transformation, and simultaneously furnish accurate energetic and mechanistic information related to that process.

Solid state phase transitions that are amenable to multiple-temperature structure investigation can be divided into two classes. The first class consists of those transitions in which the entropy change associated with the transition arises primarily from the introduction of lattice (orientational) disorder. The second class consists of those transitions in which an "internal" molecular transformation is the dominant contributor to the entropy change. These two classes of transitions differ in the nature of the high- and low-temperature limiting structures, and also in the nature of the thermodynamic and mechanistic information that can be derived from multiple-temperature structural investigation. For the first class of transitions, an increase in temperature results in conversion from an ordered to a disordered structure. In a transition of the second kind, the low-temperature limiting structure is completely ordered with all molecules in a low-energy form. The high-temperature structure is again essentially ordered, but with all molecules in a state of high internal energy. At intermediate temperatures the structure is disordered with a mixture of low-energy and high-energy molecules.

For either class of transition, to obtain useful thermodynamic information from a multiple-temperature structural investigation it is necessary to resolve the crystallographic disorder. With the resolution accomplished, thermodynamic information is available from the temperature dependence of the order parameter, dynamic information is available from the thermal parameters, and in many cases mechanistic information is implicit in the orientational relationship of the interconverting species.

In a research program now underway in this laboratory, multiple-temperature structural analyses have allowed the construction of dynamic models for several basic types of molecular transformations. Examples of each of the two classes of transitions defined above have been studied. This paper describes an investigation of the order–disorder transition in monoclinic sulfur. A preliminary description of an application of similar techniques to the spin transition in an iron(III) porphyrin complex has been communicated,[1] and an extensive series of investigations of spin transitions in aminomethylpyridine complexes of Fe(II) will be published in the near future.

Monoclinic Sulfur. To explore the utility of multiple-temperature x-ray structural techniques in the study of molecular dynamics, a system was chosen for initial investigation that met the following criteria: (1) A molecular material was required to demonstrate the applicability of the method to systems more complex than metallic alloys. (2) It was required that the material undergo a second-order phase transition with a λ point well inside the temperature range of the available x-ray equipment (100–300 K). (3) A material was required for which it would be feasible to model the energetic and mechanistic data derived from the structural investigation with relatively simple lattice energy calculations.

Thermodynamic data published by Montgomery[2] suggested that monoclinic (β) sulfur fulfilled all these criteria. These data show that monoclinic sulfur undergoes a phase transition with a λ type heat capacity anomaly at 198 K. The excess entropy associated with this transition matches that required by the disorder known to exist in the room temperature crystal structure.[3] Lattice energy calculations for this material require only a single potential function, and a good S–S potential function is available from investigations of the intermolecular vibrations in orthorhombic sulfur by Rinaldi and Pawley.[4]

The room temperature structure of monoclinic sulfur as reported by Sands[3] and more recently by Templeton and coworkers[5] is shown in Figure 1. Monoclinic sulfur at room temperature exhibits space group symmetry $P2_1/c$ with six S_8 molecules per unit cell. Since each of these S_8 molecules has the noncentrosymmetric crown configuration, two of the molecules are required to be twofold disordered. If, as Montgomery[2] suggested, the λ transition at 198 K is associated with this disorder, below the λ point the inversion center should vanish and the disorder should be gradually reduced. Disappearance of the inversion center must be accompanied by loss of either the 2_1 axis or the c glide plane. Preliminary observations in this laboratory of the systematic absences at 113 K indicated that the c glide symmetry is lost but that the 2_1 symmetry is retained. In an effort to thoroughly characterize

Table I. Summary of Experimental Parameters[a]

$\lambda = 0.71069$ Å; $2\theta_{max} = 55°$; Space group = $P2_1$; Scan mode $\theta/2\theta$; $Z = 6$; $\mu = 18.7$ cm^{-1}

Temp, K	a	b	c	β	V	Scan rate, deg/min	Scan range, deg	Crystal
113	10.799 (2)	10.684 (2)	10.663 (2)	95.71 (1)	1224.2 (4)	2.4	1.2–1.2	1
143	10.806 (2)	10.713 (2)	10.675 (2)	95.74 (2)	1229.6 (4)	2.4	1.2–1.2	1
189	10.841 (2)	10.739 (3)	10.700 (4)	95.68 (3)	1239.6 (6)	4.0	1.6–1.4	2
203	10.866 (2)	10.747 (3)	10.710 (3)	95.60 (2)	1244.7 (5)	6.0	1.6–1.4	2
218	10.876 (2)	10.763 (3)	10.720 (4)	95.64 (2)	1248.8 (6)	6.0	1.6–1.4	2
297[5]	10.926 (2)	10.855 (2)	10.790 (3)	95.92 (2)	1272.9			

Temp, K	R	R_w	$P = M_L - M_H$	EOF	No. obsd refl
113	0.022	0.027	0.984 (2)	0.97	2699
143	0.024	0.028	0.944 (2)	0.97	2658
189	0.025	0.033	0.746 (4)	1.20	2708
203	0.028	0.034	0.168 (10)	1.14	2342
218	0.027	0.033	0.136 (10)	1.09	2234

[a] In this and all subsequent tables, the estimated standard deviations of the last significant figures are given in parentheses. The scan range is given as range below $K\alpha_1$-range above $K\alpha_2$. Expressions for R and Rw are given in note 10. The symbols M_L and M_H represent the fractional occupations of the low-energy and high-energy sites, respectively; the difference, P, is a measure of the long-range order parameter in the limit of low temperature. EOF is the standard deviation in an observation of unit weight. "Observed" reflections are those with $I > 3\sigma(I)$.

the structural transition associated with the heat capacity anomaly at 198 K, five complete sets of x-ray diffraction data were collected in the range 113–218 K.

Experimental Section

Sample Preparation. Crystals of monoclinic sulfur were prepared by cooling molten sulfur (Mallinckrodt, N.F.) in a filter paper container.[6] When about half of the sulfur had crystallized, the remaining molten sulfur was poured off to expose a mass of needle-shaped crystals. Monoclinic sulfur is unstable with respect to orthorhombic sulfur below 368.4 K.[7] Crystals prepared as above transform to polycrystalline orthorhombic sulfur in less than 1 h at room temperature. If, however, the crystals are cooled below 250 K they are stable for at least several weeks. Most of the crystals examined were twinned, but with careful optical inspection it was possible to cut a fragment from a large crystal that gave no indication of twinning. The crystals used in the data collection were mounted on glass fibers, transferred to the diffractometer, and cooled immediately to below 223 K.

Data Collection. X-ray diffraction data were collected at five different temperatures with a Syntex $P\bar{1}$ diffractometer equipped with a locally constructed low-temperature apparatus[8] and a monochromatized Mo source. Two crystals were used in the data collection. The first crystal was used for the collection of the 113 and 143 K data and the second for the remaining data. The first crystal was 0.16 × 0.20 × 0.30 mm and the second 0.15 × 0.40 × 0.50 mm.

All temperature measurements were made by mounting a thermocouple in the cold stream after completion of the data collection. Care was taken to minimize heat transfer through the thermocouple leads. At the lowest temperature, temperature stability was better than ±1 °C and the measurement is probably accurate to ±2 °C. At the time these data were collected the temperature instability in the neighborhood of 200 K was ± 3 K. This temperature fluctuation arose as a result of the change in nitrogen level in the reservoir of the low-temperature apparatus, and had a period of about 1 h. Temperature measurements were averaged over several hours.

Experimental and data handling procedures used in this investigation are analogous to those described previously.[9] Lattice parameters and their estimated standard deviations were obtained from a least-squares fit of 15 automatically centered reflections. Two octants of data were collected to $2\theta_{max} = 55°$ at each temperature. Total background count time was equal to total scan count time. All data from the second crystal were corrected for absorption.[10] Because of the small size and regular shape of the first crystal, no absorption correction was applied to data from this crystal. A summary of experimental parameters is found in Table I. All data for which the intensity was greater than three times the estimated standard deviation were used in the least-squares refinement of the structure.

Refinement. Atomic positions given by Sands[3] for the disordered room temperature structure were used in the initial least-squares refinements. All refinements were carried out in the space group $P2_1$ with the 2_1 axis located at $x = 0$, $z = 1/4$, and with the constraint that the sum of the molecular occupations of the two pseudocentric sites equal one. Thus, a single parameter was refined which corresponded to the fractional occupation of one of the molecular sites. The scattering factor for sulfur was taken from the International Tables for X-Ray Crystallography.[11] The real part of the anomalous dispersion correction[12] was used in all structure factor calculations. Anisotropic thermal parameters were obtained for all atoms. In the refinement of the 113 and 143 K data, thermal parameters of the atoms in the high-energy site were fixed at the values for the corresponding atoms in the low-energy site.

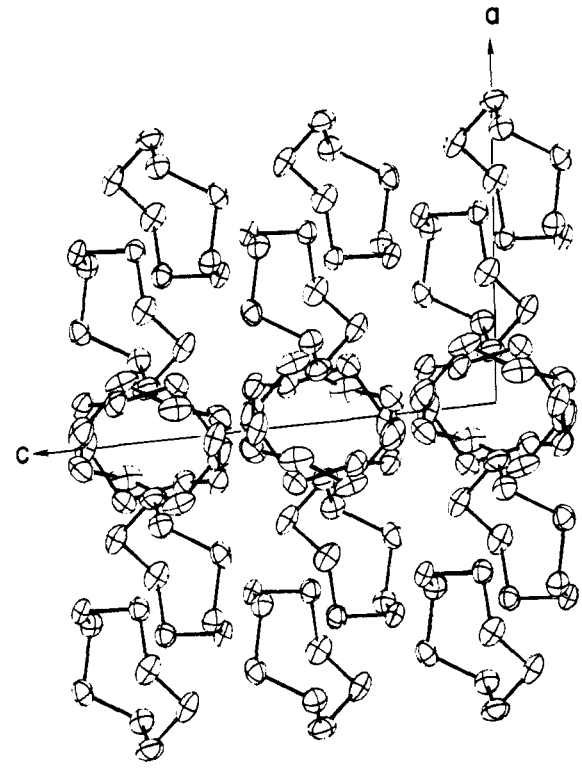

Figure 1. Packing diagram of monoclinic sulfur at room temperature projected down the b axis based on the parameters of Templeton et al.[5]. All atoms are drawn as 50% probability ellipsoids.

Table II. Final Atomic Parameters[a]

Atom	X	Y	Z	$10^4\beta_{11}$	$10^4\beta_{22}$	$10^4\beta_{33}$	$10^4\beta_{12}$	$10^4\beta_{13}$	$10^4\beta_{23}$
113 K S1	0.2239 (1)	0.5267	0.0317 (1)	35 (1)	26 (1)	39 (1)	3 (1)	0 (1)	4 (1)
S2	0.1426 (1)	0.3537 (1)	0.0081 (1)	27 (1)	38 (1)	50 (1)	−5 (1)	2 (1)	1 (1)
S3	0.2468 (1)	0.2494 (1)	−0.1039 (1)	38 (1)	35 (1)	33 (1)	−3 (1)	−9 (1)	−5 (1)
S4	0.3642 (1)	0.1390 (1)	0.0121 (1)	40 (1)	21 (1)	44 (1)	−4 (1)	−3 (1)	0 (1)
S5	0.5342 (1)	0.2254 (1)	0.0349 (1)	30 (1)	29 (1)	28 (1)	2 (1)	2 (1)	−1 (1)
S6	0.5493 (1)	0.3134 (1)	0.2070 (1)	37 (1)	31 (1)	21 (1)	0 (1)	−2 (1)	3 (1)
S7	0.5086 (1)	0.4990 (1)	0.1778 (1)	32 (1)	26 (1)	31 (1)	−4 (1)	0 (1)	−2 (1)
S8	0.3250 (1)	0.5253 (1)	0.2049 (1)	38 (1)	35 (1)	29 (1)	1 (1)	8 (1)	−6 (1)
S9	−0.2407 (1)	−0.5310 (1)	−0.0197 (1)	33 (1)	32 (1)	31 (1)	4 (1)	3 (1)	1 (1)
S10	−0.1611 (1)	−0.3576 (2)	0.0034 (1)	25 (1)	47 (1)	44 (1)	−7 (1)	0 (1)	4 (1)
S11	−0.2690 (1)	−0.2512 (1)	0.1103 (1)	41 (1)	33 (1)	35 (1)	−1 (1)	−12 (1)	−2 (1)
S12	−0.3816 (1)	−0.1424 (1)	−0.0114 (1)	43 (1)	25 (1)	39 (1)	−5 (1)	−10 (1)	3 (1)
S13	−0.5518 (1)	−0.2283 (1)	−0.0406 (1)	30 (1)	29 (1)	27 (1)	3 (1)	1 (1)	−1 (1)
S14	−0.5602 (1)	−0.3197 (1)	−0.2110 (1)	32 (1)	30 (1)	23 (1)	0 (1)	−2 (1)	1 (1)
S15	−0.5203 (1)	−0.5049 (1)	−0.1773 (1)	30 (1)	27 (1)	33 (1)	−4 (1)	2 (1)	−2 (1)
S16	−0.3352 (1)	−0.5307 (1)	−0.1968 (1)	33 (1)	39 (1)	30 (1)	4 (1)	5 (1)	−7 (1)
S17	0.1765 (1)	−0.1168 (2)	0.0870 (1)	26 (1)	42 (1)	53 (1)	3 (1)	−5 (1)	0 (1)
S18	0.0438 (1)	−0.0791 (2)	0.2072 (1)	46 (1)	41 (1)	39 (1)	3 (1)	0 (1)	17 (1)
S19	0.0020 (1)	0.1079 (2)	0.1917 (1)	54 (1)	42 (1)	28 (1)	7 (1)	−6 (1)	−1 (1)
S20	−0.1597 (1)	0.1278 (2)	0.0756 (1)	34 (1)	46 (1)	32 (1)	10 (1)	11 (1)	5 (1)
S21	−0.1175 (1)	0.1729 (1)	−0.1016 (1)	36 (1)	31 (1)	28 (1)	4 (1)	1 (1)	5 (1)
S22	−0.1245 (1)	0.0102 (2)	−0.2034 (1)	39 (1)	47 (1)	34 (1)	7 (1)	−7 (1)	−11 (1)
S23	0.0559 (1)	−0.0497 (2)	−0.2054 (1)	45 (1)	50 (1)	39 (1)	8 (1)	14 (1)	0 (1)
S24	0.0887 (1)	−0.1898 (1)	−0.0764 (1)	38 (1)	29 (1)	57 (1)	0 (1)	0 (1)	−4 (1)
S25	−0.1790 (157)	0.1022 (192)	−0.1021 (178)	27	42	53	4	−5	0
S26	−0.0718 (218)	0.0787 (227)	−0.2112 (218)	47	41	39	3	0	17
S27	0.0113 (178)	−0.1082 (191)	−0.2084 (161)	54	41	29	7	−6	−1
S28	0.1343 (162)	−0.1131 (189)	−0.1009 (160)	35	46	32	10	11	5
S29	0.1329 (161)	−0.1875 (179)	0.1019 (158)	36	31	28	4	1	5
S30	0.1437 (166)	0.0081 (195)	0.1948 (166)	39	48	34	7	−7	−11
S31	0.0043 (175)	0.0430 (198)	0.2418 (164)	45	50	39	7	14	0
S32	−0.0851 (189)	0.1292 (192)	0.0964 (188)	38	29	57	0	0	−4
143 K S1	0.2244 (1)	0.5267	0.0321 (1)	45 (1)	33 (1)	48 (1)	4 (1)	1 (1)	4 (1)
S2	0.1432 (1)	0.3543 (2)	0.0084 (1)	33 (I)	47 (1)	64 (1)	−8 (1)	1 (1)	3 (1)
S3	0.2471 (1)	0.2502 (2)	−0.1037 (1)	49 (1)	45 (1)	43 (1)	−4 (1)	−11 (1)	−5 (1)
S4	0.3641 (1)	0.1402 (2)	0.0122 (1)	53 (1)	26 (1)	54 (1)	−6 (1)	−5 (1)	0 (1)
S5	0.5341 (1)	0.2260 (2)	0.0350 (1)	39 (1)	36 (1)	35 (1)	5 (1)	3 (1)	−3 (1)
S6	0.5492 (1)	0.3136 (2)	0.2068 (1)	45 (1)	36 (1)	27 (1)	0 (1)	−3 (1)	4 (1)
S7	0.5085 (1)	0.4987 (2)	0.1779 (1)	43 (1)	33 (1)	38 (1)	−6 (1)	2 (1)	−4 (1)
S8	0.3257 (1)	0.5252 (2)	0.2050 (1)	49 (1)	42 (1)	36 (1)	2 (1)	11 (1)	−8 (1)
S9	−0.2406 (1)	−0.5301 (1)	−0.0207 (1)	39 (1)	40 (1)	42 (1)	7 (1)	3 (1)	2 (1)
S10	−0.1608 (1)	−0.3577 (2)	0.0023 (1)	30 (1)	57 (1)	57 (1)	−10 (1)	0 (1)	6 (1)
S11	−0.2680 (1)	−0.2514 (2)	0.1090 (1)	53 (1)	41 (1)	41 (1)	−1 (1)	−15 (1)	−5 (1)
S12	−0.3809 (1)	−0.1425 (2)	−0.0119 (1)	57 (1)	30 (1)	50 (1)	−6 (1)	−13 (1)	2 (1)
S13	−0.5508 (1)	−0.2281 (2)	−0.0403 (1)	40 (1)	38 (1)	34 (1)	4 (1)	2 (1)	−1 (1)
S14	−0.5597 (1)	−0.3190 (2)	−0.2106 (1)	42 (1)	40 (1)	27 (1)	0 (1)	−4 (1)	3 (1)
S15	−0.5201 (1)	−0.5037 (2)	−0.1774 (1)	36 (1)	31 (1)	42 (1)	−6 (1)	1 (1)	−3 (1)
S16	−0.3353 (1)	−0.5299 (2)	−0.1974 (1)	41 (1)	49 (1)	37 (1)	3 (1)	8 (1)	−10 (1)
S17	0.1765 (1)	−0.1161 (2)	0.0869 (1)	32 (1)	53 (1)	71 (1)	4 (1)	−8 (1)	1 (1)
S18	0.0444 (1)	−0.0779 (2)	0.2070 (1)	61 (1)	52 (1)	48 (1)	2 (1)	0 (1)	21 (1)
S19	0.0028 (1)	0.1087 (2)	0.1913 (1)	70 (1)	50 (1)	35 (1)	8 (1)	−9 (1)	−1 (1)
S20	−0.1591 (1)	0.1282 (2)	0.0760 (1)	41 (1)	58 (1)	40 (1)	12 (1)	12 (1)	6 (1)
S21	−0.1176 (1)	0.1727 (2)	−0.1012 (1)	44 (1)	42 (1)	35 (1)	6 (1)	0 (1)	5 (1)
S22	−0.1246 (1)	0.0101 (2)	−0.2023 (1)	48 (1)	63 (1)	45 (1)	8 (1)	−10 (1)	−15 (1)
S23	0.0554 (1)	−0.0494 (2)	−0.2049 (1)	53 (1)	62 (1)	50 (1)	9 (1)	19 (1)	−1 (1)
S24	0.0885 (1)	−0.1890 (2)	−0.0756 (1)	45 (1)	34 (1)	76 (1)	0 (1)	0 (1)	−7 (1)
S25	−0.1852 (39)	0.1050 (48)	−0.0761 (46)	32	53	71	4	−8	1
S26	−0.0680 (53)	0.0584 (52)	−0.2036 (45)	61	52	48	2	0	21
S27	−0.0075 (47)	−0.1174 (50)	−0.1943 (40)	70	50	35	8	−9	−1
S28	0.1497 (42)	−0.1342 (49)	−0.0880 (40)	41	58	40	12	12	6
S29	0.1293 (42)	−0.1765 (47)	0.1045 (38)	44	42	35	6	0	5
S30	0.1240 (42)	−0.0114 (49)	0.2026 (41)	48	63	45	8	−10	−15
S31	−0.0265 (44)	0.0354 (55)	0.2152 (43)	53	62	50	9	19	−1
S32	−0.1058 (50)	0.1653 (50)	0.0887 (50)	46	34	76	0	0	−7
189 K S1	0.2265 (1)	0.5267	0.0316 (1)	61 (1)	45 (1)	65 (1)	6 (1)	0 (1)	5 (1)
S2	0.1461 (1)	0.3550 (2)	0.0084 (1)	49 (1)	63 (1)	84 (1)	−11 (1)	1 (1)	3 (1)
S3	0.2497 (1)	0.2510 (2)	−0.1030 (1)	71 (1)	59 (1)	57 (1)	−7 (1)	−18 (1)	−7 (1)
S4	0.3663 (1)	0.1412 (2)	0.0128 (1)	74 (1)	35 (1)	72 (1)	−8 (1)	−9 (1)	1 (1)
S5	0.5355 (1)	0.2272 (2)	0.0361 (1)	55 (1)	45 (1)	46 (1)	5 (1)	5 (1)	−3 (1)
S6	0.5499 (1)	0.3145 (2)	0.2069 (1)	62 (1)	48 (1)	39 (1)	0 (1)	−8 (1)	5 (1)
S7	0.5095 (1)	0.4989 (2)	0.1778 (1)	60 (1)	42 (1)	52 (1)	−10 (1)	0 (1)	−6 (1)

Table II (*Continued*)

Atom	*X*	*Y*	*Z*	$10^4\beta_{11}$	$10^4\beta_{22}$	$10^4\beta_{33}$	$10^4\beta_{12}$	$10^4\beta_{13}$	$10^4\beta_{23}$
189 K S8	0.3273 (1)	0.5252 (2)	0.2045 (1)	69 (1)	55 (1)	49 (1)	2 (1)	13 (1)	−12 (1)
S9	−0.2391 (1)	−0.5283 (1)	−0.0230 (1)	56 (1)	51 (1)	57 (1)	9 (1)	5 (1)	4 (1)
S10	−0.1594 (1)	−0.3566 (2)	−0.0005 (1)	45 (1)	75 (1)	74 (1)	−12 (1)	−4 (1)	8 (1)
S11	−0.2655 (1)	−0.2506 (2)	0.1070 (1)	76 (1)	51 (1)	56 (1)	−5 (1)	−23 (1)	−5 (1)
S12	−0.3790 (1)	−0.1424 (2)	−0.0124 (1)	77 (1)	39 (1)	67 (1)	−11 (1)	−17 (1)	3 (1)
S13	−0.5482 (1)	−0.2277 (2)	−0.0398 (1)	58 (1)	48 (1)	46 (1)	6 (1)	4 (1)	−2 (1)
S14	−0.5584 (1)	−0.3178 (1)	−0.2100 (1)	57 (1)	50 (1)	37 (1)	0 (1)	−5 (1)	3 (1)
S15	−0.5183 (1)	−0.5022 (2)	−0.1779 (1)	55 (1)	40 (1)	56 (1)	−9 (1)	2 (1)	−4 (1)
S16	−0.3347 (1)	−0.5282 (2)	−0.1987 (1)	63 (1)	59 (1)	51 (1)	3 (1)	9 (1)	−13 (1)
S17	0.1769 (1)	−0.1133 (2)	0.0861 (2)	50 (1)	68 (2)	102 (2)	5 (1)	−14 (1)	2 (1)
S18	0.0461 (1)	−0.0756 (2)	0.2066 (1)	91 (2)	69 (2)	66 (1)	1 (1)	−3 (1)	27 (1)
S19	0.0044 (2)	0.1103 (2)	0.1904 (1)	102 (2)	68 (2)	48 (1)	7 (1)	−13 (1)	−1 (1)
S20	−0.1580 (2)	0.1289 (2)	0.0770 (1)	62 (1)	73 (1)	54 (1)	15 (1)	16 (1)	6 (1)
S21	−0.1179 (1)	0.1725 (2)	−0.1004 (1)	64 (1)	53 (1)	47 (1)	7 (1)	1 (1)	11 (1)
S22	−0.1247 (2)	0.0102 (2)	−0.2004 (1)	67 (1)	84 (2)	59 (1)	6 (1)	−12 (1)	−19 (1)
S23	0.0542 (1)	−0.0487 (2)	−0.2042 (1)	76 (1)	85 (2)	66 (1)	7 (1)	23 (1)	−5 (1)
S24	0.0881 (2)	−0.1875 (2)	−0.0752 (2)	65 (1)	47 (1)	105 (2)	0 (1)	0 (1)	−10 (1)
S25	−0.1835 (7)	0.1090 (12)	−0.0775 (10)	15 (6)	102 (13)	102 (11)	13 (7)	−27 (6)	0 (10)
S26	−0.0567 (11)	0.0649 (12)	−0.2057 (9)	68 (10)	88 (12)	56 (9)	29 (9)	−13 (7)	21 (8)
S27	−0.0097 (11)	−0.1153 (11)	−0.1881 (9)	95 (11)	64 (11)	58 (9)	0 (10)	−27 (8)	−13 (8)
S28	0.1530 (10)	−0.1326 (12)	−0.0806 (9)	61 (8)	85 (12)	54 (8)	21 (10)	22 (7)	−5 (8)
S29	0.1236 (9)	−0.1716 (11)	0.0994 (8)	47 (8)	67 (10)	52 (8)	3 (8)	−13 (6)	0 (7)
S30	0.1300 (8)	−0.0092 (11)	0.1976 (8)	39 (7)	90 (11)	57 (8)	25 (8)	−10 (5)	−14 (8)
S31	−0.0488 (10)	0.0470 (14)	0.2082 (9)	50 (8)	100 (13)	55 (9)	27 (9)	11 (7)	−13 (9)
S32	−0.0948 (10)	0.1799 (12)	0.0776 (11)	43 (8)	62 (10)	121 (12)	10 (8)	−9 (8)	−46 (9)
203 K S1	0.2327 (2)	0.5267	0.0295 (2)	74 (2)	55 (3)	72 (3)	9 (2)	−3 (2)	5 (2)
S2	0.1522 (2)	0.3533 (4)	0.0062 (3)	52 (2)	74 (3)	100 (3)	−16 (2)	−6 (2)	16 (2)
S3	0.2559 (2)	0.2508 (4)	−0.1043 (2)	81 (2)	61 (2)	69 (3)	−2 (2)	−19 (2)	−2 (2)
S4	0.3711 (2)	0.1409 (3)	0.0141 (3)	79 (2)	32 (2)	89 (3)	−7 (2)	−17 (2)	5 (2)
S5	0.5399 (2)	0.2268 (3)	0.0374 (2)	76 (2)	57 (2)	48 (3)	10 (2)	5 (2)	−8 (2)
S6	0.5531 (2)	0.3157 (3)	0.2077 (2)	71 (2)	52 (2)	42 (2)	2 (2)	−8 (2)	−2 (2)
S7	0.5114 (2)	0.4995 (4)	0.1780 (2)	68 (2)	45 (2)	60 (2)	−6 (2)	−3 (2)	−8 (2)
S8	0.3308 (2)	0.5257 (4)	0.2031 (2)	77 (2)	64 (2)	59 (3)	4 (2)	17 (2)	−13 (2)
S9	−0.2340 (2)	−0.5270 (1)	−0.0259 (2)	65 (2)	55 (3)	69 (3)	7 (2)	5 (2)	9 (2)
S10	−0.1547 (2)	−0.3574 (4)	−0.0047 (3)	57 (2)	87 (3)	82 (3)	−12 (2)	−2 (2)	0 (2)
S11	−0.2605 (2)	−0.2500 (4)	0.1044 (2)	91 (2)	64 (3)	60 (3)	−13 (2)	−30 (2)	−10 (2)
S12	−0.3750 (2)	−0.1428 (4)	−0.0123 (3)	96 (2)	48 (2)	64 (3)	−17 (2)	−13 (2)	1 (2)
S13	−0.5433 (2)	−0.2284 (3)	−0.0384 (2)	56 (2)	49 (2)	57 (3)	0 (2)	3 (2)	2 (2)
S14	−0.5548 (2)	−0.3166 (3)	−0.2089 (2)	66 (2)	58 (2)	41 (2)	−4 (2)	−6 (2)	12 (2)
S15	−0.5157 (2)	−0.5010 (4)	−0.1777 (2)	64 (2)	46 (2)	61 (3)	−16 (2)	6 (2)	−5 (2)
S16	−0.3315 (2)	−0.5270 (4)	−0.2007 (2)	73 (2)	65 (2)	54 (2)	2 (2)	10 (2)	−14 (2)
S17	0.1777 (4)	−0.1096 (6)	0.0865 (5)	57 (4)	66 (5)	121 (6)	5 (4)	−29 (4)	4 (4)
S18	0.0504 (5)	−0.0722 (6)	0.2065 (5)	93 (6)	87 (6)	81 (6)	21 (5)	−8 (4)	36 (4)
S19	0.0058 (6)	0.1125 (6)	0.1900 (4)	120 (6)	67 (5)	48 (5)	17 (5)	−28 (4)	−11 (4)
S20	−0.1566 (4)	0.1276 (6)	0.0789 (4)	51 (4)	76 (5)	51 (4)	17 (4)	8 (3)	−7 (4)
S21	−0.1183 (4)	0.1718 (5)	−0.0987 (4)	57 (4)	61 (4)	59 (4)	15 (3)	8 (3)	15 (3)
S22	−0.1251 (4)	0.0117 (6)	−0.1995 (4)	66 (4)	98 (5)	45 (3)	1 (4)	−17 (3)	−17 (3)
S23	0.0513 (4)	−0.0476 (7)	−0.2059 (4)	69 (4)	102 (6)	58 (4)	13 (4)	26 (3)	−9 (4)
S24	0.0898 (5)	−0.1879 (6)	−0.0728 (5)	84 (6)	47 (4)	127 (6)	−1 (4)	−14 (4)	−6 (4)
S25	−0.1808 (6)	0.1107 (9)	−0.0797 (7)	50 (5)	107 (8)	110 (8)	9 (6)	−3 (5)	5 (7)
S26	−0.0497 (8)	0.0718 (8)	−0.2053 (7)	121 (10)	84 (8)	68 (8)	−10 (7)	−9 (6)	30 (6)
S27	−0.0073 (8)	−0.1117 (9)	−0.1885 (7)	105 (8)	99 (9)	68 (8)	−7 (7)	−7 (6)	2 (7)
S28	0.1557 (7)	−0.1327 (10)	−0.0778 (7)	89 (7)	105 (9)	82 (8)	20 (8)	36 (6)	26 (7)
S29	0.1207 (6)	−0.1724 (8)	0.1014 (6)	98 (7)	68 (7)	54 (6)	−5 (6)	−19 (5)	7 (5)
S30	0.1289 (6)	−0.0055 (8)	0.1965 (7)	69 (6)	92 (8)	98 (7)	16 (6)	−10 (5)	−31 (6)
S31	−0.0532 (7)	0.0486 (10)	0.2039 (8)	95 (8)	106 (10)	107 (10)	0 (7)	22 (6)	−7 (7)
S32	−0.0899 (6)	0.1814 (8)	0.0782 (7)	49 (6)	67 (6)	125 (9)	7 (5)	14 (5)	−30 (6)
218 K S1	0.2333 (3)	0.5267	0.0302 (3)	85 (3)	54 (3)	81 (3)	6 (2)	1 (3)	7 (2)
S2	0.1529 (3)	0.3525 (5)	0.0059 (3)	68 (3)	80 (3)	110 (4)	−15 (3)	−9 (3)	13 (3)
S3	0.2558 (3)	0.2509 (5)	−0.1038 (3)	101 (3)	72 (3)	65 (3)	−5 (3)	−26 (3)	−8 (3)
S4	0.3725 (3)	0.1409 (4)	0.0147 (3)	80 (3)	36 (2)	99 (3)	−8 (2)	−16 (2)	3 (2)
S5	0.5412 (3)	0.2266 (4)	0.0382 (3)	82 (3)	50 (3)	52 (3)	7 (2)	0 (2)	−7 (2)
S6	0.5524 (3)	0.3152 (4)	0.2072 (3)	82 (3)	56 (3)	43 (2)	−4 (2)	−10 (2)	3 (2)
S7	0.5116 (3)	0.4995 (4)	0.1779 (2)	78 (3)	53 (3)	57 (3)	−16 (2)	−2 (2)	−12 (2)
S8	0.3306 (3)	0.5246 (4)	0.2027 (3)	85 (3)	73 (3)	56 (3)	−2 (3)	15 (2)	−11 (3)
S9	−0.2333 (3)	−0.5263 (1)	−0.0260 (3)	66 (3)	65 (3)	70 (3)	12 (2)	2 (2)	7 (2)
S10	−0.1540 (3)	−0.3581 (5)	−0.0056 (3)	48 (2)	94 (4)	86 (3)	−15 (3)	1 (2)	4 (3)
S11	−0.2599 (3)	−0.2507 (5)	0.1041 (3)	85 (3)	64 (3)	71 (3)	−14 (3)	−27 (2)	−4 (3)
S12	−0.3735 (3)	−0.1435 (4)	−0.0119 (3)	109 (3)	54 (3)	64 (3)	−19 (3)	−17 (2)	3 (2)
S13	−0.5415 (3)	−0.2290 (4)	−0.0376 (3)	57 (2)	64 (3)	62 (3)	4 (2)	9 (2)	0 (2)

Table II (*Continued*)

Atom	*X*	*Y*	*Z*	$10^4\beta_{11}$	$10^4\beta_{22}$	$10^4\beta_{33}$	$10^4\beta_{12}$	$10^4\beta_{13}$	$10^4\beta_{23}$
218 K S14	−0.5552 (3)	−0.3170 (4)	−0.2092 (3)	66 (2)	66 (3)	47 (2)	3 (2)	−7 (2)	8 (2)
S15	−0.5154 (3)	−0.5004 (4)	−0.1779 (3)	63 (2)	48 (3)	75 (3)	−8 (2)	8 (2)	−2 (2)
S16	−0.3320 (3)	−0.5276 (4)	−0.2011 (3)	78 (3)	66 (3)	66 (3)	8 (2)	15 (2)	−18 (2)
S17	0.1762 (5)	−0.1088 (8)	0.0860 (7)	59 (4)	97 (7)	142 (8)	4 (5)	−45 (4)	−5 (6)
S18	0.0528 (6)	−0.0721 (7)	0.2050 (5)	119 (7)	115 (7)	67 (5)	30 (6)	−14 (5)	47 (4)
S19	0.0062 (7)	0.1133 (7)	0.1878 (5)	122 (7)	69 (6)	61 (5)	14 (6)	−20 (5)	−5 (5)
S20	−0.1590 (5)	0.1266 (8)	0.0782 (5)	52 (4)	95 (6)	67 (5)	20 (5)	17 (3)	6 (5)
S21	−0.1188 (5)	0.1714 (6)	−0.1000 (4)	82 (6)	74 (5)	47 (4)	−4 (4)	6 (4)	20 (4)
S22	−0.1245 (6)	0.0114 (7)	−0.2006 (5)	74 (5)	120 (7)	56 (5)	15 (5)	−9 (4)	−28 (4)
S23	0.0505 (6)	−0.0482 (8)	−0.2057 (5)	99 (6)	111 (8)	56 (4)	12 (6)	8 (4)	−8 (5)
S24	0.0894 (6)	−0.1895 (7)	−0.0725 (6)	99 (7)	50 (4)	134 (7)	−2 (4)	−8 (5)	0 (4)
S25	−0.1828 (6)	0.1107 (9)	−0.0810 (8)	56 (5)	83 (8)	113 (8)	14 (6)	11 (5)	10 (6)
S26	−0.0472 (8)	0.0711 (8)	−0.2064 (8)	103 (9)	73 (7)	99 (8)	−21 (6)	0 (6)	16 (6)
S27	−0.0086 (10)	−0.1109 (11)	−0.1913 (8)	127 (11)	108 (10)	64 (7)	−5 (9)	−24 (8)	−4 (7)
S28	0.1518 (8)	−0.1336 (11)	−0.0795 (8)	99 (8)	87 (9)	72 (7)	11 (7)	17 (6)	0 (7)
S29	0.1198 (7)	−0.1715 (8)	0.0981 (7)	77 (7)	63 (7)	85 (8)	25 (6)	−19 (6)	0 (6)
S30	0.1294 (8)	−0.0068 (10)	0.1948 (8)	72 (7)	94 (8)	88 (7)	−3 (6)	−15 (5)	−13 (6)
S31	−0.0531 (7)	0.0485 (10)	0.2041 (8)	72 (7)	119 (11)	123 (9)	5 (7)	58 (6)	−17 (8)
S32	−0.0906 (7)	0.1787 (8)	0.0800 (8)	58 (7)	65 (6)	144 (9)	7 (5)	11 (6)	−43 (6)

[a] Anisotropic thermal parameters defined by $\exp\{-(\beta_{11}h^2 + \beta_{22}k^2 + \beta_{33}l^2 + 2\beta_{12}hk + 2\beta_{13}hl + 2\beta_{23}kl)\}$. The large standard deviations in the parameters for S25–S32 at low temperature result from the low occupation of this site (see Table I).

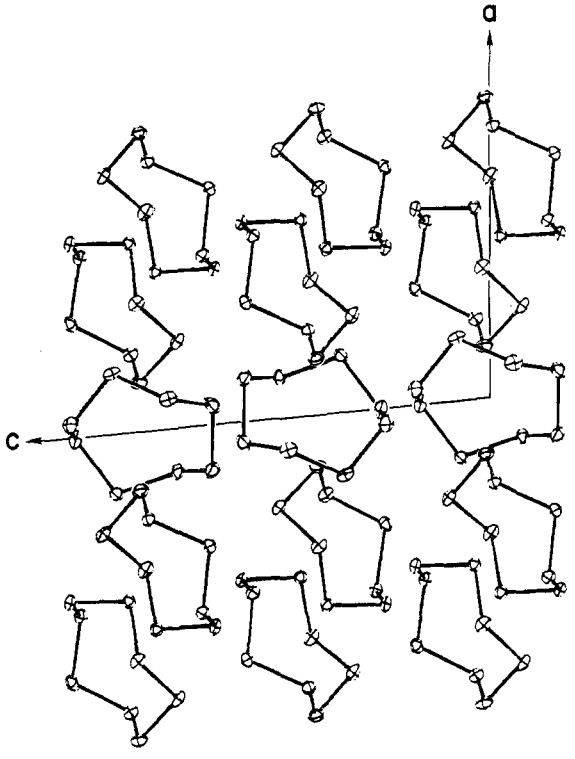

Figure 2. Packing diagram of monoclinic sulfur at 113 K projected down the *b* axis. All atoms are drawn as 50% probability ellipsoids.

A summary of *R* values and refined occupational parameters appears in Table I. Final atomic parameters are tabulated in Table II and a summary of bond distances, angles, and torsional angles is given in Table III. A packing diagram based on the 113 K parameters is shown in Figure 2. The molecule in the high-energy site (occupation = 0.01) is omitted from this figure to distinguish the ordered structure from the disordered structure shown in Figure 1.

Results and Discussion

Description of the Structure. The crystallographic data over the entire temperature range were successfully fitted to a simple two-site model for the disorder. While the disorder of the molecules in the pseudocentric sites should lead to some disorder in the two other crystallographically independent molecules, no significant evidence of such disorder is observed in the refinement. The four independent molecules exhibit small but significant distortions from idealized S_8 symmetry. The principal distortion observed in all of the independent molecules is a slight flattening of the ring. This is illustrated in the first ring by S(1)–S(4) and S(8)–S(5) distances of 4.422 (2) and 4.413 (2) Å compared to S(2)–S(7) and S(3)–S(6) distances of 4.459 (2) and 4.469 (2) Å, respectively, at 113 K. This same asymmetry is reflected in the torsional angles. Similar distortions were observed by Pawley and Rinaldi[13] in the structure of orthorhombic sulfur. The small decrease in the average S–S distance with increasing temperature (see Table III) is probably a consequence of molecular libration.

Energetics of the Transition. As can be seen in Figures 1 and 2, the principal intermolecular interaction responsible for the *difference* in energy between the two pseudocentric sites is an interaction among symmetry related molecules. This fact requires that the transition be cooperative in the sense that the energy difference between the two sites available to a particular molecule depends on the orientations of its neighbors. In the ordered (low temperature) limit, the cooperativity can be ignored and the energy difference between the alternate sites obtained experimentally from the temperature dependence of the site populations. Alternatively the temperature dependence of the observed disorder can be analyzed in terms of a mean-field model.

In the Bragg–Williams model[14] of cooperative order–disorder transitions, the energy of the system is expressed in terms of a long-range order parameter, *P*, which corresponds to the difference in the fractional occupations of the two sites, and an ordering energy, *U*, which corresponds to the difference in energy between the two sites in the otherwise ordered structure. The entropy is a function of *P* alone. This model neglects the effects of short-range order and the variation of *U* associated with the temperature dependence of the lattice parameters. Minimization of the free energy with respect to the order parameter results in the expression

$$\frac{R \ln\left(\frac{1+P}{1-P}\right)}{P} = \frac{U}{T}$$

This expression predicts a temperature dependence of *P* shown in Figure 3 and provides a convenient form in which to represent the temperature dependence of the experimentally determined order parameter. Below the critical temperature,

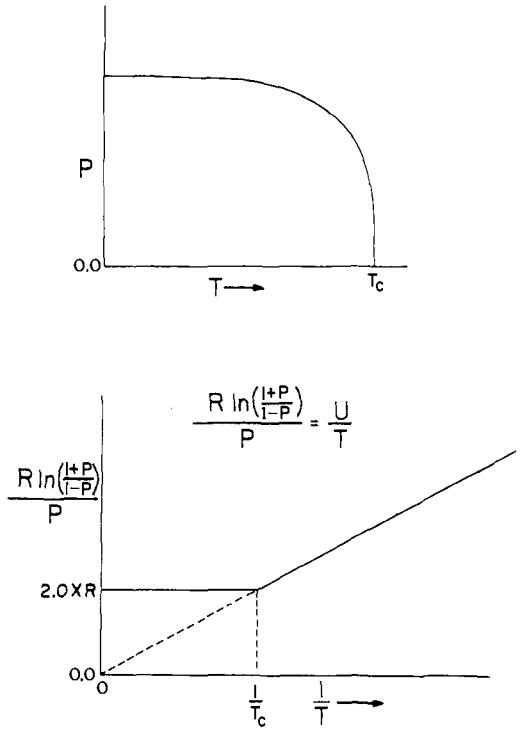

Figure 3. The temperature dependence of the long-range order parameter, P, based on the Bragg-Williams model.

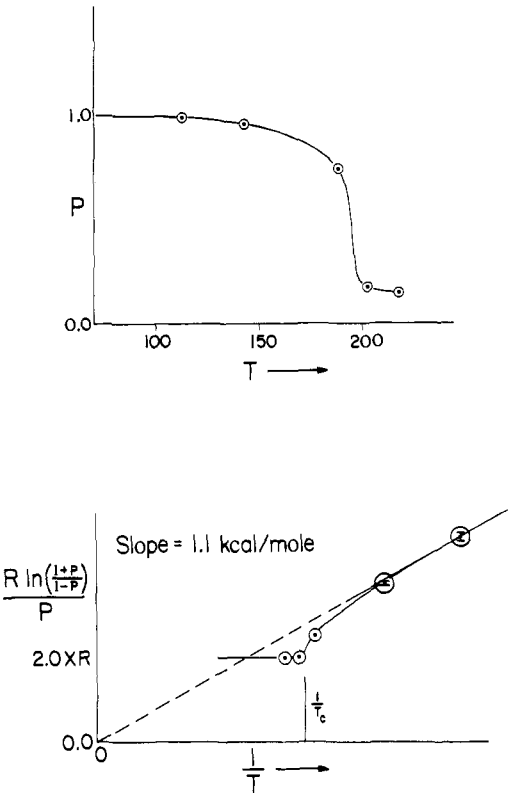

Figure 4. Temperature dependence of observed difference between the occupations of the alternate molecular orientations. In the limit of low temperature this difference is a good measure of the long-range order.

$\ln (1 + P/1 - P)/P$ vs. $1/T$ is linear with slope U/R. Above the critical temperature, $P = 0.0$ and $\ln (1 + P/1 - P)/P = 2.0$. In the low-temperature limit the difference between the occupations of the two molecular sites obtained in the crystallographic refinement is a good measure of the long-range order parameter.

A plot of the observed $\ln (1 + P/1 - P)/P$ in Figure 4 shows the expected dependence on $1/T$ in the limit of low temperature. The slope of this plot gives an ordering energy $U = 1.1$ kcal/mol. (1.1 kcal/N_0 is the energy necessary to move one molecule of S_8 from the low-energy site to the high-energy site in the otherwise ordered structure.) As the critical temperature is approached, the plot deviates from the Bragg-Williams limit. The neglect of short-range order and the temperature dependence of the lattice parameters can both be invoked to account for this deviation. The value of $1/T_c$ indicated on this plot corresponds to the thermodynamically measured λ point.[2] This is clearly a convenient representation since one can examine the fit to the Bragg-Williams model, and obtain both the ordering energy and the critical temperature from the same plot.

Lattice Energy Calculations. In an effort to model the 1.1 kcal/mol ordering energy obtained from the crystallographic investigation, several lattice energy calculations have been carried out with the PCK6 program written by Williams.[15] The potential function used for these calculations was that obtained by Rinaldi and Pawley.[4]

All calculations were based on a sphere of 10 Å radius containing 530 atoms and centered at the crystallographic origin. Interactions between atoms more than 6.0 Å apart were neglected. In these calculations only the position and orientation of the S_8 molecule at the origin were refined. As a test of the refinement procedure the potential energy was calculated for the molecule at the origin in the ordered structure; the position and orientation of this molecule were then refined to minimize the lattice energy. This refinement resulted in a decrease of 0.13 kcal/mol in the potential energy with shifts in the position and orientation of less than 0.04 Å and 4°.

To minimize the effect of the rather large uncertainties associated with the atomic positions of the molecule in the high-energy site at 113 K, lattice energy calculations for this molecule were based on initial coordinates obtained by inversion of the molecule in the low-energy site. Refinements of the position and orientation of the molecules in the low-energy and high-energy sites provided an estimate of the energy difference between these two sites of 2.6 kcal/mol. This energy difference represents a calculated upper bound on the ordering energy U. Refinement of the position and orientation of the eight neighboring molecules and of internal distortions of the molecule would certainly result in a calculated ordering energy closer to the experimental value of 1.1 kcal. On the other hand, because of the uncertainties associated with the parametrization of the potential function and the assumption of additive, isotropic, pairwise interactions between atoms, such a calculation is probably not justified.

Lattice energy calculations of this type based on the structural data at higher temperature would be much more difficult. In the presence of a significant amount of disorder, both the structural and thermodynamic observables are averages over many local configurations. Energy calculations thus would require either experimental or theoretical determination of the short-range order, and could not depend completely upon crystallographically determined atomic positions.

The Barrier to the Interconversion. The primary utility of lattice energy calculations in the study of molecular phase transitions is in the exploration of the energy surface between alternate configurations. Only semiquantitative information concerning the barrier to the interconversion process is directly available from the crystallographic data.

In the case of the order-disorder transition in monoclinic sulfur, a reasonable interconversion pathway involves a simple 45° rotation of the molecule in the pseudocentric site. This process could be considered to result from an exaggerated li-

Table III. Bond Distances, Bond Angles, and Torsional Angles

Bond distances

From	To	113 K	143 K	189 K	203 K	218 K
S1	S8	2.050 (2)	2.049 (2)	2.044 (2)	2.051 (4)	2.039 (4)
S1	S2	2.050 (2)	2.050 (2)	2.054 (2)	2.063 (4)	2.075 (5)
S2	S3	2.050 (2)	2.051 (2)	2.049 (2)	2.036 (4)	2.022 (5)
S3	S4	2.054 (1)	2.050 (2)	2.053 (2)	2.065 (4)	2.076 (4)
S4	S5	2.047 (1)	2.047 (2)	2.046 (2)	2.046 (3)	2.047 (4)
S5	S6	2.054 (1)	2.051 (2)	2.047 (2)	2.052 (3)	2.040 (4)
S6	S7	2.048 (2)	2.047 (2)	2.045 (2)	2.044 (4)	2.050 (5)
S7	S8	2.051 (1)	2.046 (2)	2.044 (2)	2.026 (3)	2.031 (4)
S9	S10	2.047 (2)	2.043 (2)	2.041 (2)	2.019 (4)	2.009 (5)
S9	S16	2.056 (1)	2.054 (2)	2.055 (2)	2.059 (4)	2.069 (4)
S10	S11	2.053 (2)	2.050 (2)	2.051 (2)	2.068 (4)	2.077 (5)
S11	S12	2.050 (1)	2.049 (2)	2.046 (2)	2.033 (4)	2.025 (4)
S12	S13	2.051 (1)	2.047 (2)	2.046 (2)	2.043 (3)	2.041 (4)
S1	S14	2.057 (1)	2.056 (2)	2.056 (2)	2.051 (3)	2.062 (4)
S14	S15	2.049 (2)	2.048 (2)	2.049 (2)	2.048 (4)	2.042 (4)
S15	S16	2.048 (1)	2.049 (2)	2.044 (2)	2.059 (3)	2.055 (4)
S17	S18	2.052 (2)	2.047 (2)	2.049 (3)	2.018 (8)	1.980 (10)
S17	S24	2.054 (2)	2.053 (2)	2.052 (2)	2.053 (7)	2.053 (9)
S18	S19	2.052 (2)	2.053 (2)	2.051 (2)	2.047 (7)	2.063 (9)
S19	S20	2.048 (2)	2.046 (2)	2.046 (2)	2.036 (7)	2.054 (9)
S20	S21	2.045 (1)	2.043 (2)	2.043 (2)	2.043 (6)	2.059 (7)
S21	S22	2.047 (2)	2.047 (2)	2.042 (2)	2.029 (7)	2.030 (9)
S22	S23	2.053 (2)	2.050 (2)	2.044 (2)	2.027 (6)	2.014 (9)
S23	S24	2.040 (2)	2.041 (2)	2.040 (2)	2.088 (8)	2.101 (10)
S25	S32	1.739 (309)	1.987 (69)	1.986 (14)	2.022 (10)	2.044 (11)
S25	S26	2.272 (271)	2.012 (71)	2.090 (15)	2.094 (12)	2.134 (11)
S26	S27	2.188 (309)	1.993 (72)	2.005 (17)	2.029 (11)	2.007 (13)
S27	S28	1.667 (249)	1.955 (64)	2.016 (15)	2.044 (11)	2.032 (13)
S28	S29	2.305 (243)	2.137 (59)	2.027 (14)	2.038 (10)	2.011 (11)
S29	S30	2.310 (269)	2.060 (67)	2.034 (15)	2.061 (11)	2.051 (12)
S30	S31	1.675 (259)	1.720 (63)	2.043 (12)	2.070 (10)	2.083 (11)
S31	S32	1.971 (268)	2.065 (74)	2.025 (18)	1.976 (12)	1.948 (13)
av(S1–S16)		2.051	2.049	2.048	2.048	2.048
av(S17–S24)		2.049	2.048	2.046	2.043	2.044
av(S25–S32)		2.02	1.99	2.028	2.042	2.039

Bond angles

From	Thru	To	113 K	143 K	189 K	203 K	218 K
S8	S1	S2	106.69 (6)	106.72 (7)	106.57 (7)	106.36 (16)	106.17 (19)
S3	S2	S1	107.97 (7)	108.02 (7)	108.07 (7)	107.85 (15)	108.08 (21)
S2	S3	S4	107.64 (6)	107.54 (7)	107.59 (7)	106.83 (17)	107.01 (22)
S5	S4	S3	107.77 (6)	107.81 (7)	107.78 (7)	107.41 (16)	107.77 (20)
S6	S5	S4	107.62 (6)	107.59 (7)	107.68 (7)	107.63 (13)	107.10 (16)
S5	S6	S7	108.12 (6)	108.17 (6)	108.16 (6)	108.47 (16)	108.86 (18)
S8	S7	S6	107.88 (6)	107.98 (7)	107.93 (7)	108.43 (15)	107.85 (19)
S7	S8	S1	108.05 (6)	108.04 (7)	108.08 (7)	107.75 (14)	107.80 (18)
S10	S9	S16	105.83 (6)	105.95 (7)	106.07 (7)	106.20 (15)	106.47 (18)
S9	S10	S11	108.24 (6)	108.30 (7)	108.24 (7)	108.22 (15)	107.91 (19)
S12	S11	S10	107.23 (6)	107.44 (7)	107.53 (7)	108.05 (17)	107.93 (21)
S11	S12	S13	107.94 (7)	107.89 (7)	108.06 (7)	108.33 (16)	108.06 (21)
S12	S13	S14	107.83 (6)	107.74 (7)	107.82 (7)	107.80 (13)	108.23 (15)
S15	S14	S13	108.26 (6)	108.31 (6)	108.32 (6)	107.93 (15)	107.59 (19)
S14	S15	S16	107.63 (6)	107.64 (7)	107.86 (7)	107.49 (14)	108.08 (18)
S15	S16	S9	107.91 (6)	107.83 (7)	107.98 (7)	108.14 (14)	108.18 (18)
S18	S17	S24	108.18 (7)	108.17 (8)	108.03 (11)	108.58 (35)	109.39 (40)
S17	S18	S19	107.59 (7)	107.66 (8)	107.41 (11)	108.02 (40)	108.12 (47)
S20	S19	S18	108.50 (7)	108.38 (8)	108.34 (11)	108.18 (36)	108.17 (45)
S19	S20	S21	109.14 (7)	109.07 (8)	108.89 (11)	108.61 (32)	107.06 (40)
S22	S21	S20	106.88 (7)	106.85 (8)	106.98 (10)	107.35 (32)	107.22 (40)
S23	S22	S21	106.56 (7)	106.68 (8)	106.85 (11)	107.41 (32)	107.75 (40)
S22	S23	S24	108.83 (7)	108.70 (8)	108.69 (11)	109.32 (37)	109.88 (47)
S17	S24	S23	109.17 (7)	109.19 (8)	108.89 (11)	108.50 (36)	107.57 (45)
S32	S25	S26	112.13 (1217)	115.73 (306)	109.87 (65)	107.72 (46)	106.92 (44)
S27	S26	S25	114.96 (1417)	115.23 (327)	109.53 (81)	107.45 (58)	107.22 (57)
S26	S27	S28	109.60 (1353)	112.18 (333)	110.02 (76)	109.58 (61)	108.99 (69)
S29	S28	S27	125.19 (1253)	114.20 (289)	110.52 (71)	109.81 (51)	111.36 (62)
S28	S29	S30	94.91 (967)	108.51 (298)	108.24 (75)	106.25 (55)	107.35 (60)
S29	S30	S31	108.75 (1271)	111.37 (327)	107.35 (68)	105.56 (51)	105.62 (54)
S32	S31	S30	104.65 (1219)	118.60 (360)	109.87 (80)	107.86 (56)	108.02 (57)

Table III. (Continued)

Bond angles							
From	Thru	To	113 K	143 K	189 K	203 K	218 K
S31	S32	S25	144.26 (1306)	118.33 (331)	111.84 (84)	110.35 (59)	111.81 (59)
av(S1–S16)			107.66	107.69	107.73	107.68	107.69
av(S17–S24)			108.10	108.09	108.01	108.25	108.14
av(S25–S32)			114.	114.	109.6	108.07	108.41

Torsional angles				113 K	143 K	189 K	203 K	218 K
S1	S2	S3	S4	97.5 (1)	97.6 (1)	97.7 (1)	98.1 (2)	97.8 (2)
S2	S3	S4	S5	−98.3 (1)	−98.3 (1)	98.1 (1)	−98.7 (2)	−98.6 (2)
S3	S4	S5	S6	100.9 (1)	101.0 (1)	100.9 (1)	101.1 (2)	100.5 (2)
S4	S5	S6	S7	−99.4 (1)	−99.3 (1)	−99.4 (1)	−98.8 (2)	−99.2 (2)
S5	S6	S7	S8	96.4 (1)	96.5 (1)	96.5 (1)	96.2 (2)	96.8 (2)
S6	S7	S8	S1	−98.6 (1)	−98.6 (1)	−98.6 (1)	−98.7 (2)	−98.9 (2)
S7	S8	S1	S2	101.3 (1)	101.2 (1)	101.2 (1)	101.2 (2)	101.4 (2)
S8	S1	S2	S3	−100.0 (1)	−100.0 (1)	−100.0 (1)	−100.7 (2)	−100.6 (2)
S9	S10	S11	S12	−98.2 (1)	−98.1 (1)	−97.9 (1)	−97.4 (2)	−97.8 (2)
S10	S11	S12	S13	98.0 (1)	97.9 (1)	97.8 (1)	97.2 (2)	97.4 (2)
S11	S12	S13	S14	−100.6 (1)	−100.6 (1)	−100.6 (1)	−100.8 (2)	−101.2 (2)
S12	S13	S14	S15	98.9 (1)	99.1 (1)	98.9 (1)	99.6 (2)	99.3 (2)
S13	S14	S15	S16	−96.4 (1)	−96.5 (1)	−96.2 (1)	−96.4 (2)	−95.9 (2)
S14	S15	S16	S9	99.3 (1)	99.1 (1)	98.8 (1)	98.6 (2)	98.2 (2)
S15	S16	S9	S10	−101.6 (1)	−101.6 (1)	−101.6 (1)	−101.8 (2)	−101.5 (2)
S16	S9	S10	S11	100.5 (1)	100.5 (1)	100.5 (1)	100.2 (2)	100.3 (2)
S17	S18	S19	S20	99.8 (1)	99.9 (1)	100.2 (1)	100.0 (4)	100.1 (5)
S18	S19	S20	S21	−98.5 (1)	−98.5 (1)	−98.6 (1)	−98.8 (4)	−99.2 (5)
S19	S20	S21	S22	97.7)1)	97.6 (1)	97.4 (1)	98.4 (4)	98.6 (5)
S20	S21	S22	S23	−99.5 (1)	−99.6 (1)	−99.6 (1)	−99.4 (4)	−99.3 (5)
S21	S22	S23	S24	101.3 (1)	101.4 (1)	101.5 (1)	100.0 (4)	100.0 (5)
S22	S23	S24	S17	−98.1 (1)	−98.1 (1)	−98.1 (1)	−96.6 (4)	−96.3 (5)
S23	S24	S17	S18	95.7 (1)	95.6 (1)	95.9 (1)	95.5 (4)	95.7 (5)
S24	S17	S18	S19	−98.1 (1)	−98.1 (1)	−98.4 (1)	−98.9 (4)	−99.2 (6)
S25	S26	S27	S28	−86.0 (181)	−92.6 (40)	−98.2 (8)	−99.9 (6)	−100.4 (6)
S26	S27	S28	S29	97.0 (167)	91.9 (40)	97.0 (10)	97.3 (7)	96.6 (8)
S27	S28	S29	S30	−105.7 (159)	−91.3 (37)	−95.7 (8)	−95.6 (7)	−95.4 (8)
S28	S29	S30	S31	106.4 (122)	95.7 (38)	98.7 (8)	100.5 (6)	100.1 (6)
S29	S30	S31	S32	−90.2 (136)	−97.2 (44)	−99.9 (9)	−103.5 (7)	−102.4 (7)
S30	S31	S32	S25	71.2 (242)	85.3 (51)	96.4 (10)	99.4 (6)	98.7 (6)
S31	S32	S25	S26	−73.5 (252)	−77.0 (47)	−92.2 (10)	−95.3 (6)	−94.3 (6)
S32	S25	S26	S27	76.2 (172)	87.7 (44)	95.2 (10)	97.1 (6)	97.2 (7)

bration about the principal axis of inertia. The barrier along this libration coordinate serves as an upper bound to the minimum energy path for the transformation. Inspection of the thermal parameters of the molecule reveals no unusually large motions along the librational coordinate, either below or near the transition temperature. This indicates the presence of a barrier greater than about 0.5 kcal/mol for the high-energy to low-energy transition.

A series of lattice energy calculations, similar to those described above, was carried out in which the molecule at the origin was rotated in increments of $\pi/32$ about its principal axis of inertia. The resulting plot of potential energy vs. rotation coordinate is shown in Figure 5. The low-energy potential surface in the neighborhood of 45° was produced by rotation of the molecule in the high-energy site *after* energy minimization refinement of its position and orientation. The difference in energy between the minima at zero and $\pi/2$, 0.6 kcal, reflects the contribution of internal molecular distortions to the lattice energy. The effects of such internal distortions on the calculated energy of the high-energy site were reduced by refinement of the configuration produced by inversion rather than that produced by a 45° rotation.

These calculations place an upper bound on the barrier to the forward (low energy to high energy) transformation of about 5 kcal/mol and estimate a barrier to the reverse reaction of about 3–4 kcal/mol. These barriers are large enough to account for the small thermal parameters observed for molecules in both sites. On the other hand they are small enough

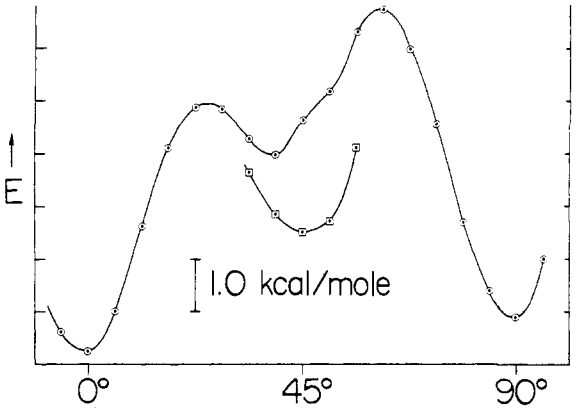

Figure 5. Calculated energy surface for rotation of a single S_8 molecule about its principal axis. The lower minimum at 45° was obtained by inversion of the molecule at 0° followed by energy minimization refinement of its position and orientation.

to account for the fact that no thermal hysteresis is observed crystallographically on a 10-min time scale; the first-order rate constant[16] corresponding to a 5 kcal barrier at 113 K is on the order of 500 s^{-1}. These calculations indicate that the pathway consisting of a simple, independent molecular rotation is at least a significant contributor to the transformation mechanism. An effort to determine experimental rate constants from nuclear quadrupole resonance data is now underway.

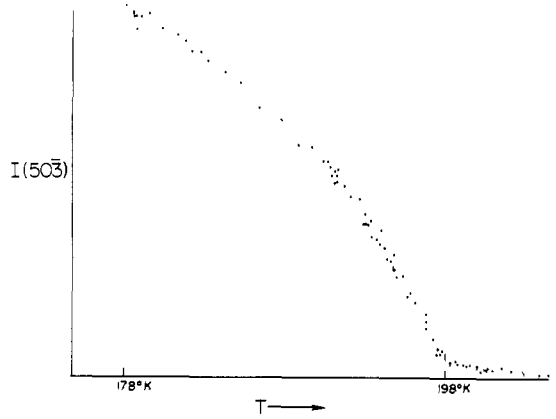

Figure 6. Intensity vs. temperature measurements for the 50$\bar{3}$ reflection.

Vibrational Analysis. The potential energy surface calculated above provides an estimate of the root mean square librational displacement of the molecule about its principal axis of about 3°.[17] As pointed out by Pawley and Rinaldi[13] in their vibrational analysis of orthorhombic sulfur, the assumption of rigid body motion is not reliable for S_8 because of the existence of several very low energy internal vibrational modes. It is, however, worthwhile to point out that thermal motion analysis of the type developed by Schomaker and Trueblood[18] gives root mean square displacements of 4, 3, and 2° about the three principal axes of libration, with the third axis corresponding most closely with the principal axis of inertia.

Critical Phenomena. The temperature dependence of the disorder in the critical region depends on the dimensionality and range of the ordering interactions.[19] Information can be obtained both from the temperature dependence of the long-range order parameter below the critical temperature and from the intensity of the critical scattering observed above the critical temperature. In monoclinic sulfur the existence of short-range order with a relatively long correlation length just above the critical temperature is reflected by the fact that in Figure 4 the plot of "P" vs. T does not go to zero in a critical fashion, but approaches zero asymptotically. It is also observed that above the critical temperature, intense reflections of the type $h0l$, $l \neq 2n$, occur without appreciable broadening. These reflections are systematically absent in the completely disordered structure.

Just below the critical temperature the intensity of reflections of the type $h0l$, $l = 2n + 1$, is expected to obey the power law $I/I_0 = B^2[(T_c - T)/T_c]^{2\beta}$ where the value of the critical exponent β depends upon the nature of the interactions responsible for the transition. If the interactions are three dimensional and long range (e.g., coulombic interactions) β is expected to be about 0.5. Three-dimensional interactions of short range (e.g., dipole–dipole or van der Waals interactions) usually produce $\beta \approx 0.3$ as predicted by the three-dimensional Ising model. In cases where the interactions are of short range, but are confined to two dimensions, β is observed to be close to the value of 0.125 predicted by the two-dimensional Ising model. Above T_c the intensity of critical scattering should be proportional to $[(T - T_c)/T]^{-\gamma}$ where γ has been shown to be 1.25 and 1.75 for the three-dimensional and two-dimensional Ising models, respectively.[20]

Since the data at five different temperatures presented in Figure 4 are not sufficient for quantitative analysis of the critical behavior, the temperature dependence of the intensity of the 50$\bar{3}$ reflection was determined in two separate experiments. Below T_c, where the intensity changes rapidly as a function of temperature, simultaneous intensity and temperature measurements were carried out with a crystal mounted directly on a copper–constantan thermocouple. The intensity was measured at 54 temperatures in the range 178–196 K (see Figure 6). Intensity measurements were also made with this arrangement above T_c, but the background scattering from the thermocouple resulted in large uncertainties in these measurements. A more reliable determination of the temperature dependence of the critical scattering was obtained by measurements of the intensity of the 50$\bar{3}$ reflection from the crystal used for collection of the three high-temperature data sets. Average intensities measured over several hours were made at four temperatures in the range 205–224 K. Temperature measurements were obtained from a calibration of temperature vs. cold stream heater voltage conducted immediately after the data collection.

Least-squares fits of 54 measurements in the range 178–196 K for T_c between 197 and 198 K gave $\beta = 0.27$–0.33 and $B = 1.2$–1.4 (with the assumption that $I_0 = I(115\ \text{K})$). The standard deviation of the critical exponent β obtained from the least-squares fits ranged from 0.003 to 0.005, but the major uncertainty in this exponent arises from uncertainty in the determination of the critical temperature. Precise determination of the critical temperature is difficult because close to T_c both Bragg scattering and critical scattering contribute significantly to the observed intensity. Fits of the four observations above T_c yield γ in the range 0.9–1.3. Uncertainty in T_c and in the background correction of the intensity measurements are the major contributors to the uncertainty in γ.

While more accurate measurements of the critical exponents β and γ are planned in conjunction with measurements of the temperature dependence of the correlation length, the preliminary measurements described above are clearly in accord with those predicted by the three-dimensional Ising model. In addition, the fit of the intensity of the 50$\bar{3}$ reflection above T_c to a power law with an exponent close to the Ising value of 1.25 provides a satisfying explanation of the behavior of the "P" vs. T curve in Figure 4. That is, "short-range" order contributes significantly to the difference in the site occupations obtained from the crystallographic refinements near T_c. The fact that both β and γ reflect three-dimensional ordering is consistent with the fact that no streaks of diffuse scattering associated with two-dimensional order are observed. While inspection of the packing diagram in Figure 4 might lead one to expect that the interactions responsible for the development of order are highly anisotropic, no experimental evidence of this anisotropy has been obtained in the current investigation. An anisotropy of the type expected may be revealed by measurements of the correlation lengths above T_c.

Conclusions

This investigation demonstrates the utility of complete multiple-temperature x-ray structural analysis in the thermodynamic and mechanistic characterization of a phase transformation in a molecular solid. While the experimental data obtained for the order–disorder transition in monoclinic sulfur provide a basis for sophisticated investigations of molecular dynamics, it is demonstrated that most of the essential features of the thermodynamics, lattice dynamics, and transition pathway can be modeled with relatively simple lattice energy calculations based on the structural data. The technique of multiple-temperature analysis as developed in this investigation promises to serve as a powerful probe in a number of important chemical and biochemical areas. Several investigations are now underway in this laboratory of iron(II) and iron(III) complexes that exhibit "spin equilibria". In one such complex, an iron(III) porphyrin is observed to transform from a low-spin six-coordinate geometry to a high-spin five-coordinate geometry; application of multiple temperature struc-

tural analysis to systems of this type can yield unique *dynamic* models of chemically significant molecular transformations.

Acknowledgments. This research was made possible by the support of the UCLA Research Committee, the UCLA Campus Computing Network, and the UCLA President's Undergraduate Research Fellowship Program. We also wish to thank Mr. Hsi-Chao Chow for his help in the initial stages of this work.

Supplementary Material Available: A listing of all observed and calculated structure factor amplitudes (45 pages). Ordering information is given on any current masthead page.

References and Notes

(1) J. P. Collman, T. N. Sorrell, K. O. Hodgson, A. K. Kulshrestha, and C. E. Strouse, *J. Am. Chem. Soc.*, **99**, 5180 (1977).
(2) R. L. Montgomery, *Science*, **184**, 562 (1974).
(3) D. E. Sands, *J. Am. Chem. Soc.*, **87**, 1395 (1965).
(4) R. P. Rinaldi and G. S. Pawley, *J. Phys. C*, **8**, 599 (1975).
(5) L. K. Templeton, D. H. Templeton, and A. Zalkin, *Inorg. Chem.*, **15**, 1999 (1976).
(6) C. E. Dull, W. O. Brooks, and H. C. Metcalfe, "Modern Chemistry", Holt and Co., New York, N.Y., 1953.
(7) B. Meyer in "Inorganic Sulfur Chemistry", G. Nickless, Ed., American Elsevier, New York, N.Y., 1968.
(8) C. E. Strouse, *Rev. Sci. Instrum.*, **47**, 871 (1976).
(9) J. Strouse, S. W. Layten, and C. E. Strouse, *J. Am. Chem. Soc.*, **99**, 562 (1977).
(10) Programs used in this work included DATred, written at UCLA; JBPATT, JBFOUR, and PEAKLIST, modified versions of Fourier programs written by J. Blount; ORFLSF, a local version of ORFLS (Busing, Martin, and Levy); ORTEP (Johnson), figure plotting; ABSORB, a modified version of ABSN (Coppens), absorption correction; parameters used in the data reduction are the same as given in A. K. Wilkerson, J. B. Chodak, and C. E. Strouse, *J. Am. Chem. Soc.*, **97**, 3000 (1975). All least-squares refinements computed the agreement factors R and R_w according to $R = \Sigma||F_o| - |F_c||/\Sigma|F_o|$ and $R_w = [\Sigma w_i||F_o| - |F_c||^2/\Sigma w_i|F_o|^2]^{1/2}$, where F_o and F_c are the observed and calculated structure factors, respectively, and $w^{1/2} = 1/\sigma(F_o)$. The parameter minimized in all refinements was $\Sigma w_i||F_o| - |F_c||^2$. All calculations were performed on the IBM 360-91KK computer operated by the UCLA Campus Computing Network.
(11) "International Tables for X-Ray Crystallography", Vol. IV, Kynoch Press, Birmingham, England, 1974, p 72 ff.
(12) D. T. Cromer and D. Liberman, *J. Chem. Phys.*, **53**, 1891 (1970).
(13) G. S. Pawley and R. P. Rinaldi, *Acta Crystallogr., Sect. B*, **28**, 3605 (1972).
(14) T. Muto and Y. Takagi, "The Theory of Order-Disorder Transitions in Alloys", Solid State Reprints, Academic Press, New York, N.Y., 1955–1956.
(15) D. E. Williams, *Acta Crystallogr., Sect. A*, **28**, 629 (1972).
(16) S. Glasstone, K. J. Laidler, and H. Eyring, "The Theory of Rate Processes", McGraw-Hill, New York, N.Y., 1941.
(17) U. Shmueli and P. A. Kroon, *Acta Crystallogr., Sect. A*, **30**, 768 (1974).
(18) V. Schomaker and K. N. Trueblood, *Acta Crystallogr., Sect. B*, **24**, 63 (1968).
(19) E. J. Samuelsen and D. Semmingsen, *Solid State Commun.*, **17**, 217 (1975), and references cited therein.
(20) R. J. Birgeneau, H. J. Guggenheim, and G. Shirane, *Phys. Rev. B*, 1, 2211 (1970), and references cited therein.

Radicals and Scavengers. 7. Diffusion Controlled Scavenging of Phenyl Radicals and Absolute Rate Constants of Several Phenyl Radical Reactions[1]

Roy G. Kryger, John P. Lorand,*[2] Neal R. Stevens, and Nelson R. Herron

Contribution from the Department of Chemistry, Boston University, Boston, Massachusetts 02215, and Filson Chemistry Laboratories, Central Michigan University, Mt. Pleasant, Michigan 48859. *February 4, 1977*

Abstract The thermal decomposition of phenylazotriphenylmethane (PAT) has been studied in mixtures of benzene and chlorobenzene with mineral oil in the presence of the phenyl radical scavengers I_2, CBr_4, $BrCCl_3$, and Me_2CHI. Greater than 90% yields of halobenzenes as scavenging products are observed at all concentrations in pure aromatic solvents, as previously reported. In viscous mixtures, however, high scavenging yields are found only at high scavenger concentrations, while at low scavenger concentrations yields fall as low as 32%. Substantial concomitant increases in benzene yield (in chlorobenzene mixtures) occur. Substitution of *n*-heptane for mineral oil almost entirely eliminates the drop in scavenging yields. These observations are readily explained by postulating that the reactions of scavengers with phenyl radicals are nearly diffusion controlled in benzene or chlorobenzene. An order of magnitude or greater increase in viscosity then decreases the diffusion rate constants significantly, allowing other reactions, particularly formation of benzene by H abstraction from mineral oil, to compete. Alternative models, e.g., complexing of scavengers with PAT or cage scavenging, do not explain the difference in behavior of mineral oil and *n*-heptane. Two predictions of this model have been fulfilled: first, the relative reactivities of scavengers toward phenyl radicals approach unity at high viscosities; second, the rate constant, k_H^{app}, for Ph· + R–H → Ph–H + R· (R–H = mineral oil) can be calculated by assigning to the I_2 and CBr_4 scavenging reactions the diffusion limited value calculated via the combined Wilke–Chang and von Smoluchowski equations. The calculated value of k_H decreases with rising viscosity to a plateau value which is essentially the same for both scavengers, viz., $k_H = 3.3 \pm 0.7 \times 10^5\ M^{-1}\ s^{-1}$. Other rate constants are calculated from competition studies. The rate constants estimated by Starnes and by MacLachlan and McCarthy, and extrapolated from gas phase results at ~300 °C of Duncan and Trotman-Dickenson are in poor agreement with the present values. The value for phenyl with O_2 is found to be virtually identical with that for CBr_4; thus the reason for the "small" ratio of 1200 for k_{O_2}/k_{CCl_4} reported by Russell and Bridger, and the *apparent* unreactivity of phenyl toward O_2, is the high reactivity of phenyl toward CCl_4 and other solvents, not a low reactivity toward O_2. The selectivity–reactivity relationship is not obeyed by several radicals, including phenyl.

The phenyl radical and its substituted analogs have been extensively studied in solution. Several means of generating them are known;[3] they have been shown to add to aromatic rings,[3] double bonds,[3] and trivalent phosphorus,[4] and sometimes probably to divalent sulfur,[5] as well as to abstract the univalent atoms H, Cl, Br, and I,[3] but to react inefficiently with O_2 in CCl_4.[6] Their relative reactivities toward a variety of substrates have been determined[7,8] and compared with those of alkyl, alkoxy, and halogen radicals.[7]

In contrast to numerous alkyl radicals[9] and the *tert*-butoxy